Supplementary Information

Near infrared II laser controlled free radical release nanogenerator for synergistic nitric oxide and alkyl radical therapy of breast cancer

Weiwei Wu[a,1], Yan Yang[b,1], Zhuoying Liang[a,1], Xiling Song[a], Yadong Huang[b,], Lin Qiu[c], Xiaozhong Qiu[d], Siming Yu[a,*], Wei Xue[a,*]*

[a] Key Laboratory of Biomaterials of Guangdong Higher Education Institutes, Guangdong Provincial Engineering and Technological Research Center for Drug Carrier Development, Department of Biomedical Engineering, Jinan University, Guangzhou 510632, China

[b] Department of Cell Biology, Guangdong Province Key Laboratory of Bioengineering Medicine, Jinan University, Guangzhou 510632, China

[c] The First Affiliated Hospital of Jinan University, Guangzhou 510632, China

[d] Guangdong Provincial Key Laboratory of Construction and Detection in Tissue Engineering, School of Basic Medical Science, Southern Medical University, Guangzhou, Guangdong 510515, China

* Corresponding authors: Yadong Huang (tydhuang@jnu.edu.cn); Siming Yu (siming_yu@hotmail.com); Wei Xue (weixue_jnu@hotmail.com)

[1] These authors contributed equally to this work.

Fig. S1 Zeta potential value of P@Lip-RGD and P(IR/BNN6/AIPH)@Lip-RGD.

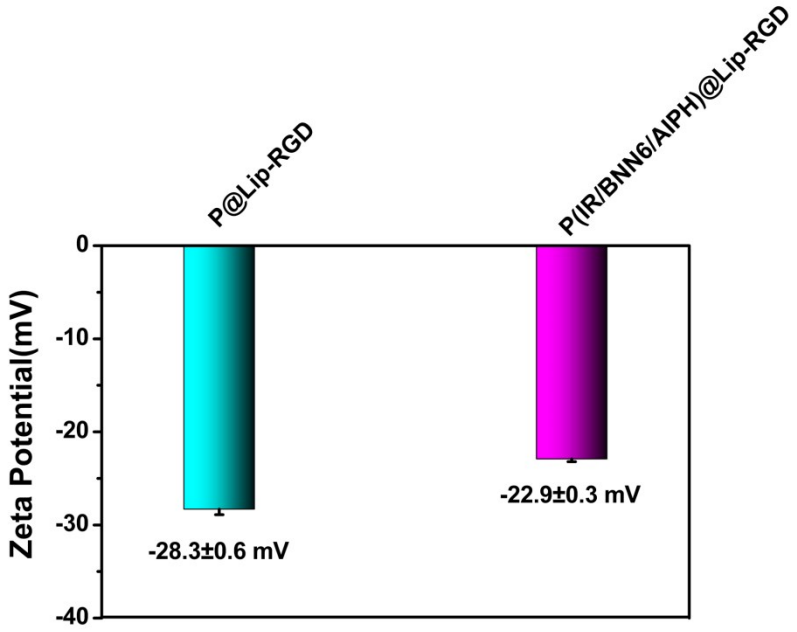

Fig. S2 Standard curves of IR1061, BNN6 and AIPH for concentration determination. Note that characteristic UV-Vis absorption peak for IR1061, BNN6 and AIPH were 1060 nm, 367 nm and 364 nm, respectively.

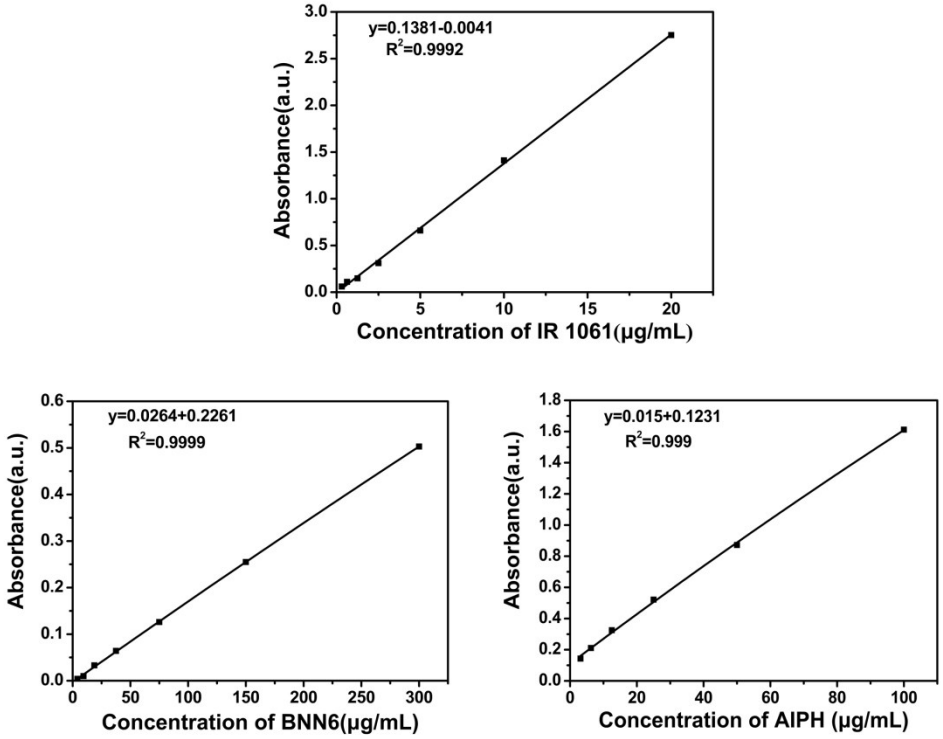

Fig. S3 Photothermal stability evaluation of P(IR/BNN6/AIPH)@Lip-RGD by repeating 5 times of heating-cooling process, using a 1064 nm laser with a power density of 0.5 W/cm^2.

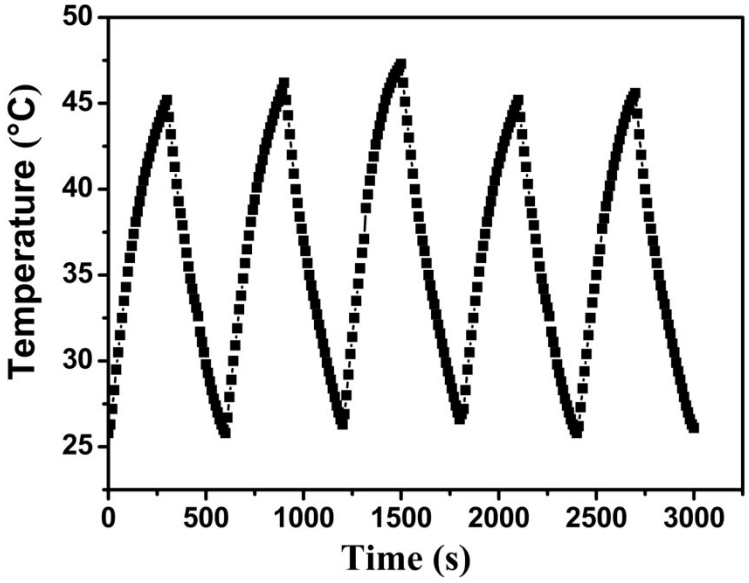

Fig. S4 Color changes of P(IR/BNN6/AIPH)@Lip-RGD dispersion under different temperatures and times in the presence of ABTS probe. Under heating conditions, AIPH can decompose to alkyl radical, which can react with ABTS to form green $ABTS^{+\bullet}$. The color intensity is proportional to the alkyl radical concentration.

Fig. S5 Stability evaluation of P(IR/BNN6/AIPH)@Lip-RGD in biologically relevant media by monitoring hydrodynamic diameter changes, over a period of 7 days.

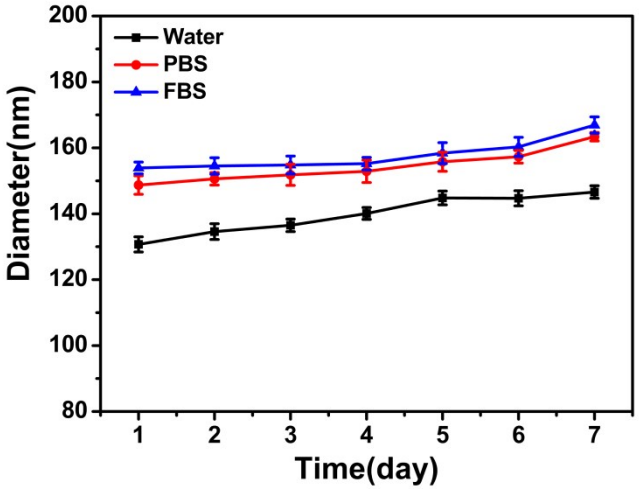

Fig. S6 Confocal images and flow cytometry measurements show the cellular uptake of P(IR/BNN6/AIPH)@Lip-RGD at an incubation time of 1h, 2h and 4h. Note that P(IR/BNN6/AIPH)@Lip-RGD and cell nucleus were stained by green FITC and blue DAPI, respectively. Scale bar represents 50 μm.

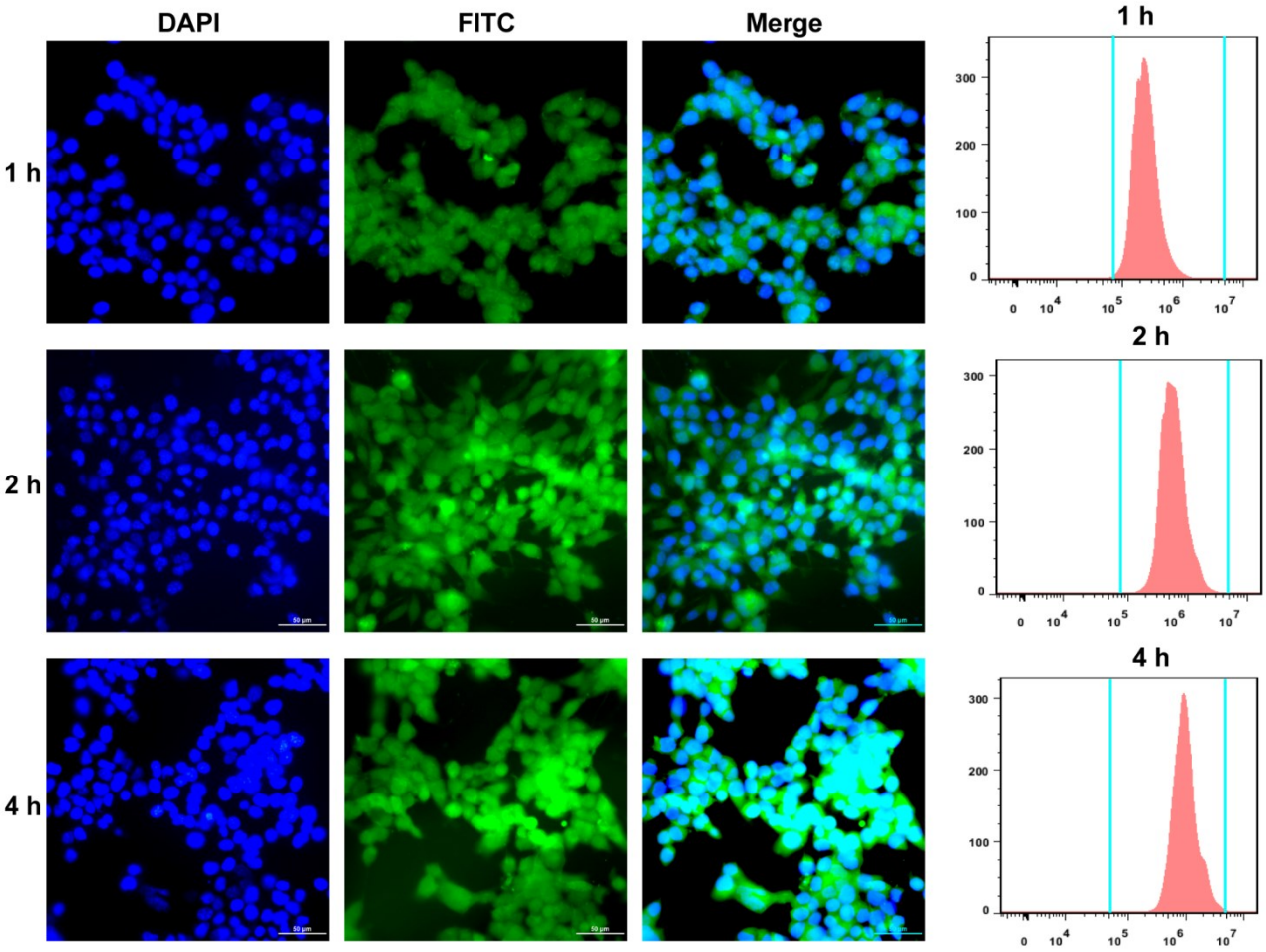

Fig. S7 Confocal images and flow cytometry measurements show the cellular uptake of P(IR/BNN6/AIPH)@Lip at an incubation time of 1h, 2h and 4h. Note that P(IR/BNN6/AIPH)@Lip and cell nucleus were stained by green FITC and blue DAPI, respectively. Scale bar represents 50 μm.

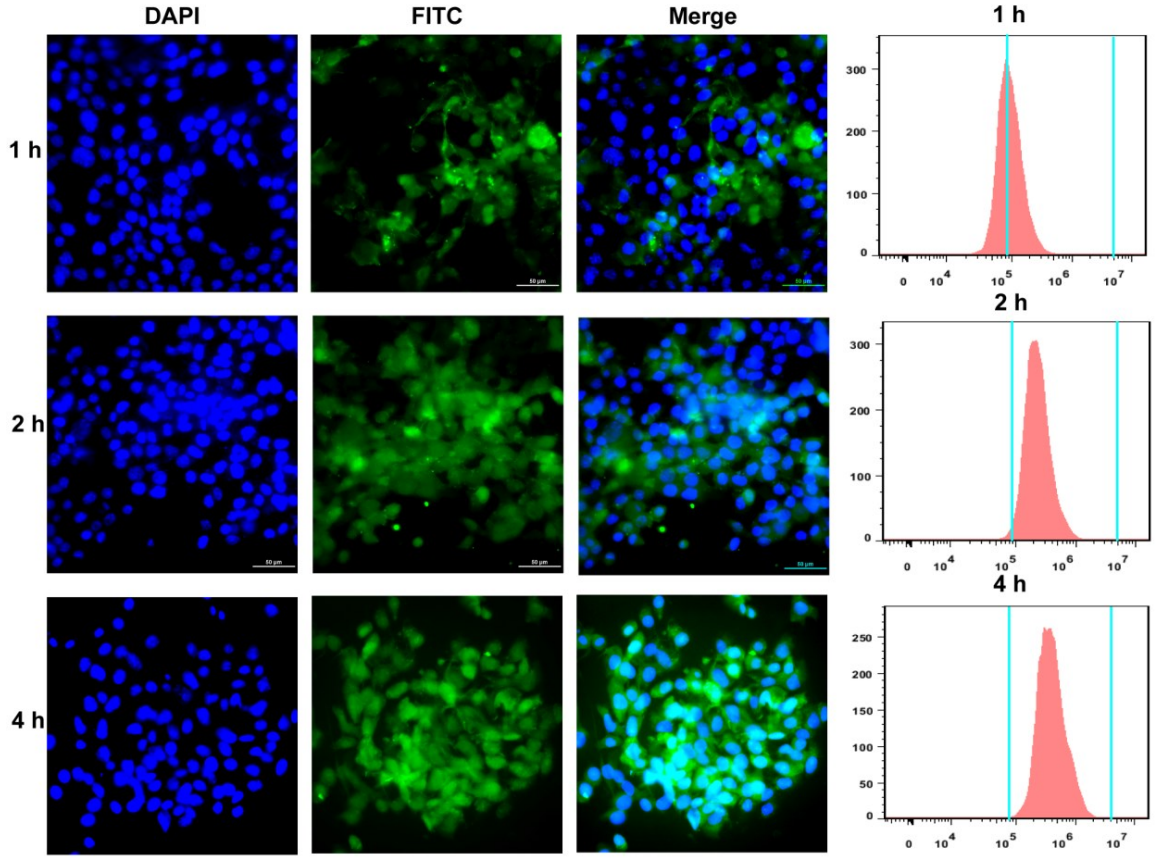

Fig. S8 Flow cytometric analysis on the intracellular NO and ROS generation level in different treating groups.

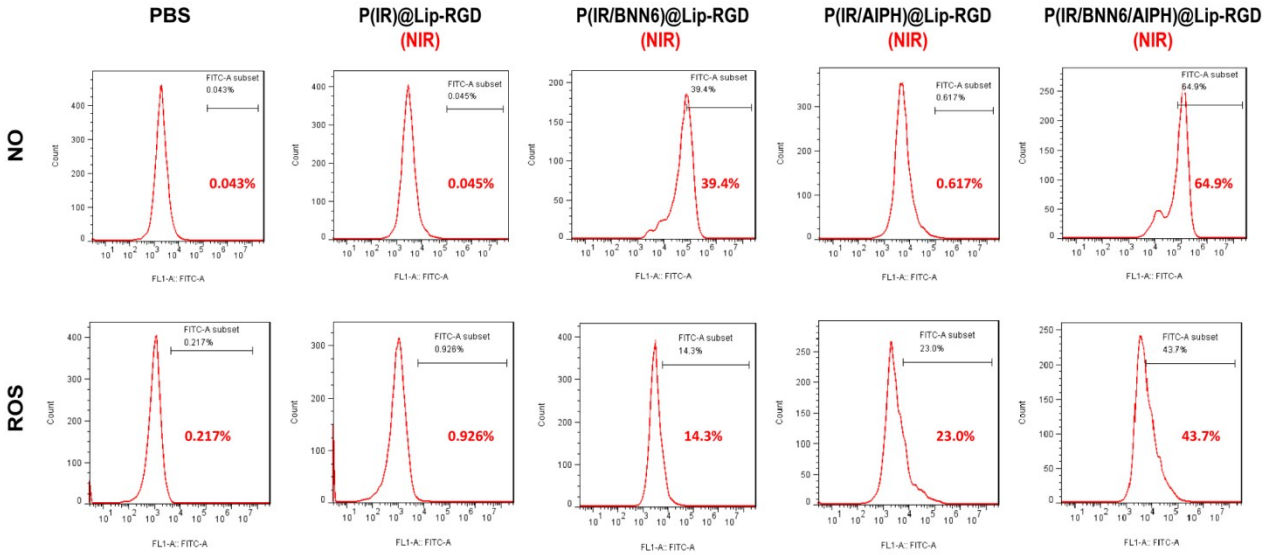

Fig. S9 *In vivo* fluorescent imaging assay of tumor-bearing nude mice. (A) Fluorescent images of mice at different times after *i.v.* injection of P(IR/BNN6/AIPH)@Lip-RGD and P(IR/BNN6/AIPH)@Lip. Black circles indicate the tumor position of mice. (B) Ex vivo fluorescent images of major organs and tumors collected from mice 6 h post-injection. (C) Changes in fluorescent intensity of tumor tissues along with time after *i.v.* injection of P(IR/BNN6/AIPH)@Lip-RGD and P(IR/BNN6/AIPH)@Lip. (D) Relative fluorescence value of tumors in different treated groups calculated by dividing the fluorescence intensity of the tumor with that of liver. (E) Quantitative analysis of fluorescent on the main organs and tumors after sacrificed at 6 h post injection. Data are presented as means ± s. d (n = 3).